Journal of Alloys and Compounds 506 (2010) 721–727

Contents lists available at ScienceDirect

Journal of Alloys and Compounds

journal homepage: www.elsevier.com/locate/jallcom

Metal halide doped metal borohydrides for hydrogen storage: The case of $Ca(BH_4)_2$–CaX_2 (X = F, Cl) mixture

Ji Youn Lee, Young-Su Lee*, Jin-Yoo Suh, Jae-Hyeok Shim, Young Whan Cho

Materials/Devices Division, Korea Institute of Science and Technology, Seoul 136-791, Republic of Korea

ARTICLE INFO

Article history:
Received 17 April 2010
Received in revised form 30 June 2010
Accepted 7 July 2010
Available online 15 July 2010

Keywords:
Hydrogen storage material
Metal borohydrides
Thermodynamic properties
Computer simulations

ABSTRACT

We have explored metal halide doping in metal borohydrides in order to modify hydrogen desorption/absorption properties of such high-capacity solid-state hydrogen storage materials. The specific application here is 10 mol% addition of CaX_2 (X = F, Cl) to $Ca(BH_4)_2$. The materials are analyzed using in-situ X-ray diffraction, differential scanning calorimetry, thermogravimetry, and IR spectroscopy, and the experimental results are compared against theoretical predictions from first-principles. Interestingly, in a fully hydrogenated state, $CaCl_2$ dissolves into $Ca(BH_4)_2$ whereas CaF_2 exists as a separate phase. During the course of dehydrogenation, CaH_2–CaF_2 solid solution, CaHCl, and a new Ca–H–Cl compound are observed. In-situ X-ray diffraction study reveals that CaX_2 interacts with $Ca(BH_4)_2$ in the early stage of decomposition, which could facilitate a direct decomposition of $Ca(BH_4)_2$ into CaH_2 and CaB_6 without forming intermediate phases such as CaB_2H_x which seem to be thermodynamically in close competition with the formation of CaH_2 and CaB_6. Our first-principles calculation estimates that the decrease in the decomposition temperature due to the CaH_2–CaX_2 interaction would be less than 10 °C, and therefore the major contribution of CaX_2 is to change the dehydrogenation pathway rather than the overall thermodynamics.

1. Introduction

Recent years has seen a great interest and advance in metal borohydride research under the hope to find a material that can store hydrogen in high volumetric and gravimetric density. Metal borohydrides indeed exhibit among the highest hydrogen storage capacity [1], but their high capacity is plagued by high thermal stability and slow hydrogen absorption and desorption kinetics. For that reason, experimental and theoretical efforts have been put forth to overcome these difficulties; the strategies taken so far are to add catalysts, to design thermodynamically destabilized systems, to synthesize mixed cation compounds, to confine materials in nanoporous scaffolds, etc. [2–6].

Another recent approach is to adjust thermodynamics of a metal borohydride ($M(BH_4)_n$) by mixing with halides of the same kind of metal (MX_n) [7,8], a representative case being $LiBH_4$–LiCl. There are several intriguing aspects in $M(BH_4)_n$–MX_n system such as solid solution formation [4,9,10] and change in ion mobility [11]; all of these could affect hydrogen desorption and absorption properties in one way or another. To elaborate more, we take F^- ion substitution as an example. The dehydrogenated products of metal borohydrides ($M(BH_4)_n$) mostly include respective metal hydrides (MH_n), and interestingly enough these metal hydrides could form a solid solution with metal fluorides (MF_n) [12–14]. There is also a possibility of F replacing H in metal borohydrides. Indeed, this type of substitution has been previously investigated for $LiBH_4$ [10] and for alanates like $NaAlH_4$ and Na_3AlH_6 [15–18].

One important aspect of the anion substitution concerns an extensive use of transition metal halides as a precursor of catalysts [4,19–21]. A metathesis reaction between transition metal chloride and alkali metal borohydride would irreversibly produce alkali metal chloride, e.g., $3LiBH_4 + TiCl_3 \rightarrow 3LiCl + Ti(BH_4)_3$. This reaction scheme is actually the most common method of synthesizing transition metal borohydrides [5,22,23]. Previous studies have seen unintentional doping of LiCl generated by such a scheme into $LiBH_4$ when $TiCl_3$ catalyst is used [24,25], and recently Mosegaard et al. provided a direct evidence of dissolution of LiCl into $LiBH_4$ [9]. The formation of a solid solution will certainly affect the stability of a metal borohydride and this effect deserves a separate attention in order to isolate the catalytic effect of a transition metal element itself.

Although earlier theoretical results hold promise for such an anion substitution as a way to adjust thermodynamics [10,16], combined experimental and theoretical studies are needed before this method is seriously pursued. Formation of solid solutions or new compounds, accompanying enthalpy and free energy change,

* Corresponding author. Tel.: +82 2 958 5412; fax: +82 2 958 5379.
E-mail address: lee0su@kist.re.kr (Y.-S. Lee).

0925-8388/$ – see front matter © 2010 Elsevier B.V. All rights reserved.
doi:10.1016/j.jallcom.2010.07.051

and reaction pathway would be the important points of discussion. In this work, we investigate CaX_2 (X = F, Cl) doping effect on $Ca(BH_4)_2$. $Ca(BH_4)_2$ is one of the representative reversible metal borohydrides [21,26]. It exhibits 9.6 wt% of hydrogen storage capacity upon dehydrogenation through the following reaction:

$$Ca(BH_4)_2 \leftrightarrow \frac{2}{3}CaH_2 + \frac{1}{3}CaB_6 + \frac{10}{3}H_2. \quad (1)$$

The phase composition and the hydrogen desorption behavior of the mixtures, $Ca(BH_4)_2 + CaX_2$, were investigated by X-ray diffraction (XRD), differential scanning calorimetry (DSC), and thermogravimetry (TG) together with a density functional theory (DFT) study.

2. Experimental

The starting materials are $Ca(BH_4)_2$ (assay 98%, Sigma–Aldrich), CaF_2 (assay 99.5+%, Sigma–Aldrich), $CaCl_2$ (assay 95%, Kanto), and CaH_2 (assay 99.9%, Sigma–Aldrich). Water from hygroscopic $CaCl_2$ was removed by heating the powder up to 200 °C and holding it for 8 h in vacuum. $Ca(BH_4)_2$, CaF_2, and CaH_2 were used as-purchased. The powders were handled in an argon-filled glove box (LABstar, MBraun, $p(O_2, H_2O) < 1$ ppm) whenever necessary.

Two mixtures were prepared: $0.9Ca(BH_4)_2 + 0.1CaF_2$ (sample **1**) and $0.9Ca(BH_4)_2 + 0.1CaCl_2$ (sample **2**) in molar ratio. For each mixture, about 1 g of powder was ball-milled with seven 12.7 mm and fourteen 7.9 mm diameter Cr-steel balls. The ball milling was conducted using a planetary mill (Fritsch P7) at 600 rpm for 4 h. The as-milled mixtures were heat treated at 300 °C for 12 h to allow equilibration. In order to suppress decomposition of $Ca(BH_4)_2$ at elevated temperatures, about 10 bar of H_2 pressure was applied during the heat treatment. The same treatment procedure was applied to pure $Ca(BH_4)_2$. The heat treated samples were used for further analysis.

In order to investigate the formation of a solid solution or a compound between CaH_2 and CaF_2 (or $CaCl_2$), three compositions were chosen where the mole fraction of CaF_2 (x_F) is 0.25, 0.5, or 0.75, and that of $CaCl_2$ (x_{Cl}) is 0.07, 0.14, or 0.25. The same ball-milling condition was applied and the mixtures were then heat treated at 450 °C for 12 h under 10 bar of H_2 pressure.

Differential scanning calorimetry (Netzsch DSC 204 F1) and thermogravimetric analysis (Netzsch TG 209 F1) were carried out to locate thermal events and the accompanying mass change. For the DSC and TG analysis, ca. 1–3 mg of sample was used and the samples were heated up to 500 °C at a scanning rate of 2 °C/min under flowing Ar (assay 99.9999%, 50 ml/min).

Laboratory X-ray diffraction data were collected using a Bruker D8 Advance X-ray diffractometer (Cu Kα radiation, λ = 1.5418 Å). The measurements were carried out at room temperature. A borosilicate glass capillary of $\varphi = 0.7$ mm was used as a sample holder.

In-situ synchrotron XRD data were collected at the 10B·XRS KIST-PAL beamline in Pohang Accelerator Laboratory. The selected X-ray wavelength was 0.80023 Å. A MAR345 image plate detector was used and the FIT2D program [27] was employed to integrate 2-D images. A sapphire tube (O.D. = 1.52 mm, I.D. = 1.07 mm) was used as a sample holder. Temperature was raised at a rate of 10 °C/min up to 300 °C and then 1 °C/min up to 500 °C. An XRD pattern was collected every 137 s. The hydrogen pressure was maintained at 2 bar throughout the in-situ measurements.

FT-IR spectra were collected using Bruker ALPHA FT-IR spectrometer. The measurements were done in an argon-filled glove box.

3. Computational

Total energies of pure $Ca(BH_4)_2$, CaH_2, CaF_2, $CaCl_2$, CaHCl, etc. were estimated in the framework of density functional theory. Specifically, Perdew–Burke–Ernzerhof generalized gradient approximation was adopted for exchange-correlation functional [28], and planewave pseudopotential method was used [29]. All the calculations were done using Quantum-ESPRESSO package [30,31] and the ultrasoft pseudopotential [32]. A planewave cutoff of 50 Ry and a charge density cutoff of 400 Ry were used. Number of *k*-points was chosen such that the total energy converges within 1 meV/atom. The lattice parameters and the atomic positions were fully relaxed for all the calculations. Two concentrations were tested for the anion substitution where one or two $[BH_4]$ units (or H) are substituted by Cl (or F) in the $\sqrt{2} \times \sqrt{2} \times 2$ supercell of β-$Ca(BH_4)_2$ containing 8 formula units (88 atoms). The enthalpy and entropy of several compounds were obtained within the harmonic approximation; phonon density of states were calculated based on density functional perturbation theory [33] as implemented in the Quantum-ESPRESSO package. Details of the calculations are summarized in Table S1 in the supplementary data.

4. Results and discussion

4.1. Phase compositions of starting material

In the $Ca(BH_4)_2$–CaX_2 system, two types of substitution can take place. One is substitution of the whole $[BH_4]^-$ unit by Cl^- or F^- and the other is substitution of H in $[BH_4]^-$ by F (Cl would not likely to replace H due to the size difference). The reaction energies summarized in Table 1 give a rough measure on whether this type of substitution would take place or not. The numbers are 0 K limit without zero point energy. In the case of the whole substitution as in reactions (a) and (b), substitution by Cl^- is energetically much favored compared to F^-. It turns out that the small positive enthalpy of mixing in the reaction (b) can be overcome by the configurational entropy term, ΔS_{mix}, as temperature increases. The molar entropy of mixing of a regular solution is given as,

$$\Delta S_{mix} = -2R(x \ln x + (1-x)\ln(1-x)), \quad (2)$$

where R is the gas constant, x is the mole fraction of $CaCl_2$, and the factor 2 comes in since there are two moles of anion position per one mole of solid solution. At 25 °C and $x = 0.1$, $T\Delta S_{mix}$ is as large as 1.6 kJ/mol, which overtakes the positive enthalpy term. The large positive enthalpy of mixing in (a), on the other hand, cannot be compensated by this entropy of mixing. The difference between F and Cl is due to the fact that Cl^- behaves more closely to $[BH_4]^-$ both in terms of size and electronegativity. Molar volume of $CaCl_2$ is smaller by ca. 20%, but that of CaF_2 is smaller by ca. 60% compared to $Ca(BH_4)_2$. The ionic radii of F^- and Cl^- are 1.33 Å and 1.81 Å [34], respectively, and that of $[BH_4]^-$ is 1.9 Å being slightly larger than Cl^- [35,36]. When Cl^- (or F^-) replaces $[BH_4]^-$, charge projection on Löwdin orthonormalized atomic orbitals [37] gives a net charge of −0.43 (or −0.66); $[BH_4]^-$ has −0.49 in pure $Ca(BH_4)_2$, again confirming similarity between $[BH_4]^-$ and Cl^-.

Partial substitution by F in $[BH_4]^-$ as in reaction (c) is even more unlikely to happen. We would like to note that the large positive enthalpy change predicted by the present work contradicts to the previous study by Yin et al. [10], where spontaneous incorporation of F in $LiBH_4$ was predicted. The main difference comes from the choice of a reference state of F. We use CaF_2 in order to be consis-

Table 1
Chemical reactions that could generate or decompose X-substituted $Ca(BH_4)_2$. ΔE is per mol of $Ca((BH_4)_{1-x}X_x)_2$ or $Ca(BH_{4-x}F_x)_2$, and ΔV is the molar volume change of these with respect to pure $Ca(BH_4)_2$. Details can be found in Table S2 in the supplementary data.

Reaction	$x = 0.0625$		$x = 0.125$	
	ΔE (kJ/mol)	ΔV (%)	ΔE (kJ/mol)	ΔV (%)
(a) $(1-x)Ca(BH_4)_2 + xCaF_2 \rightarrow Ca((BH_4)_{1-x}F_x)_2$	7.4	0.4	10.9	−3.7
(b) $(1-x)Ca(BH_4)_2 + xCaCl_2 \rightarrow Ca((BH_4)_{1-x}Cl_x)_2$	0.4	−1.8	0.5	−2.5
(c) $Ca(BH_4)_2 + xCaF_2 \rightarrow Ca(BH_{4-x}F_x)_2 + xCaH_2$	18.2	1.7	33.6	2.8
(d) $Ca(BH_4)_2 + xF_2 \rightarrow Ca(BH_{4-x}F_x)_2 + xH_2$	−42.7	–	−88.2	–
(e) $Ca(BH_{4-x}F_x)_2 \rightarrow (1-x)Ca(BH_4)_2 + xCaF_2 + 2x\alpha\text{-}B + 3xH_2$	−5.4	–	−7.9	–

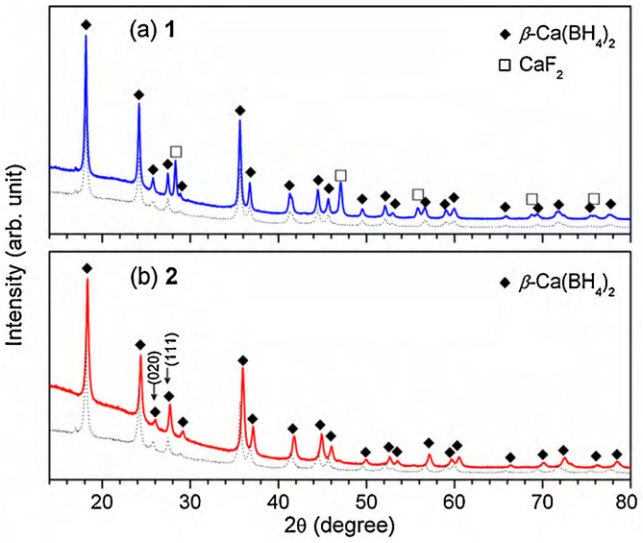

Fig. 1. XRD data of (a) **1** and (b) **2**. Dotted lines are XRD data of pure $Ca(BH_4)_2$. While CaF_2 exists as a separate phase, $CaCl_2$ completely dissolves into the lattice of β-$Ca(BH_4)_2$ resulting in a slightly reduced molar volume.

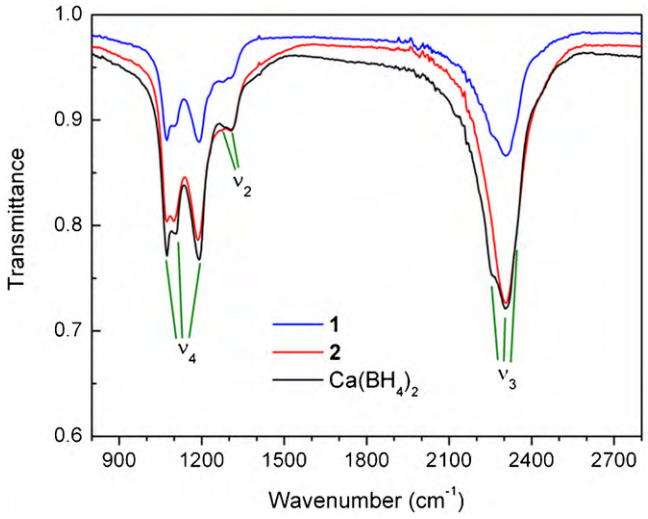

Fig. 2. FT-IR spectra of **1** (blue), **2** (red), and pure $Ca(BH_4)_2$ (black). Asymmetric bending, symmetric bending, asymmetric stretching modes of $[BH_4]^-$ are labelled as ν_4, ν_2, ν_3, respectively. (For interpretation of the references to color in this figure legend, the reader is referred to the web version of the article.)

tent with our experimental condition while F_2 was chosen instead in their calculations. When F_2 is chosen as a reference as in reaction (d), an exothermic reaction is predicted also in our calculation. However, even one succeeds making $Ca(BH_{4-x}F_x)_2$ by employing a different synthetic route, it is not likely to be thermodynamically stable since decomposition into $Ca(BH_4)_2$, CaF_2, α-B, and H_2 would spontaneously occur as in reaction (e).

The experimental results indeed corroborate our DFT ones. XRD data of **1** ($0.9Ca(BH_4)_2 + 0.1CaF_2$) and **2** ($0.9Ca(BH_4)_2 + 0.1CaCl_2$) are presented in Fig. 1. Sample **1** (top panel) is composed of two individual phases, $Ca(BH_4)_2$ and CaF_2, meaning no chemical reaction between the two. The volume per formula unit (f.u.) is 103.8 Å^3/f.u., which is the same as pure $Ca(BH_4)_2$ (black dotted line) In contrast, **2** (bottom panel) is composed of a single phase β-$Ca(BH_4)_2$: no peaks from $CaCl_2$ are found. Apparently, the peaks of β-$Ca(BH_4)_2$ are systematically shifted toward higher angles with respect to the corresponding peaks of pure $Ca(BH_4)_2$. In addition, change in relative intensities of the peaks can be immediately noticed, e.g., between (0 2 0) and (1 1 1) peak. All of these serve as direct evidences of dissolution of $CaCl_2$ in β-$Ca(BH_4)_2$. Even the volume decrease by ca. 2.6% (101.1 Å^3/f.u.) matches quite well with the DFT results under similar doping concentration (see Table 1). The decrease in volume is also consistent with the ordering in the aforementioned ionic radii ($Cl^- < [BH_4]^-$). The partial substitution by F might be better detected by IR spectroscopy than XRD if the substitution does not occur extensively. Fig. 2 shows FT-IR spectra of **1**, **2**, and pure $Ca(BH_4)_2$. The measured FT-IR spectra agree well with a previous report [38] and do not clearly show any new IR active modes that can be assigned to the vibration modes of $[BH_{4-n}F_n]^-$ ($n = 1$–4), confirming very limited substitution effect of F in $Ca(BH_4)_2$, if any.

This limited substitution makes a good contrast with a solid solution formation in CaH_2–CaF_2 system [39]. One of the reasons lies in a different character of H in $Ca(BH_4)_2$ and in CaH_2. The effective radius of H strongly depends on the charge state: a neutral H atom would be as small as the Bohr radius (0.53 Å) but the radius of H anion can be as big as 2.1 Å [40]. The similarity between H and F holds when H is anionic as in alkali or alkaline earth metal hydrides: calculated lattice parameters of CaF_2 and CaH_2 are 5.509 Å and 5.428 Å, respectively, differing only by 4.5% in volume. On the other hand, the effective charge of H in $Ca(BH_4)_2$ is about −0.33 [41,42] and it is covalently bonded to B. The size difference between H and F in such a bonding state is indeed manifested by the volume difference: the volume per formula unit of $Ca(BF_4)_2$ is 138.2 Å^3 [43], which is about 30% larger than that of $Ca(BH_4)_2$. Another reason lies in the different coordination environment. In $Ca(BF_4)_2$, a single F atom bridges between Ca and B, and the average ∠Ca–F–B angle of the first coordination shell is 151° [43], but in $Ca(BH_4)_2$, two H atoms in average bridge between Ca and B showing average ∠Ca–H–B of 102°. When H is substituted by F, $[BH_3F]^-$ would rotate to change the coordination environment, which will bring an additional distortion in the structure on top of the size difference and will increase the energy of the system. The overall result certainly is a negligible substitution effect of F in $Ca(BH_4)_2$.

4.2. Decomposition reaction

We present in Fig. 3 DSC data of **1** and **2**. The absence of the phase transformation peaks around 150 °C [44,45] is due to the fact that $Ca(BH_4)_2$ has already transformed into the high temperature polymorph during the ball milling and the heat treatment as is seen in

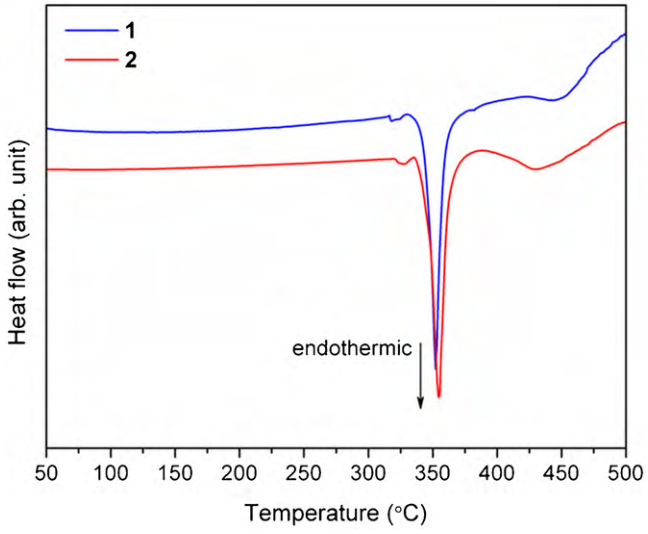

Fig. 3. Differential scanning calorimetry data of **1** (blue) and **2** (red). (For interpretation of the references to color in this figure legend, the reader is referred to the web version of the article.)

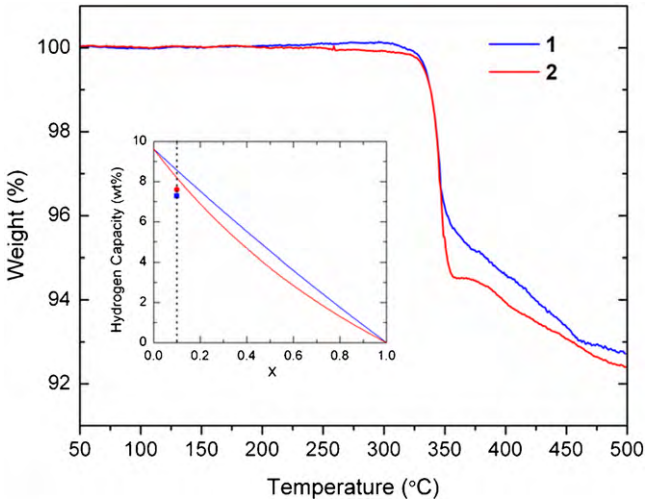

Fig. 4. Thermogravimetry data of **1** (blue) and **2** (red). Theoretical hydrogen capacity as a function of the mole fraction of CaX_2 (solid lines) is shown in the inset together with the experimental values (filled circles). (For interpretation of the references to color in this figure legend, the reader is referred to the web version of the article.)

Fig. 1. The addition of CaF_2 or $CaCl_2$ does not introduce any irreversible chemical reactions: all the thermal events recorded here are endothermic. The main endothermic peak at ca. 350 °C and the subsequent smaller peak at higher temperature appear similar to the DSC profile of pure $Ca(BH_4)_2$ [46].

Thermogravimetry data are shown in Fig. 4. In the inset, the theoretical and the experimental total weight loss as a function of the mole fraction of CaX_2 are plotted. The capacity loss with respect to pure $Ca(BH_4)_2$ is unavoidable since we add an inert compound which does not contain hydrogen at all. The difference in weight profile between **1** and **2** is noteworthy. The distinct multistep decomposition behavior is due to the intermediate phase(s) consistently reported by several previous work [46–48]. The more abrupt drop in the weight in **2** could be associated with a different decomposition pathway. In order to elucidate this point, we have carried out in-situ synchrotron XRD measurements.

4.3. In-situ synchrotron X-ray diffraction

Fig. 5 shows in-situ XRD data of **1** at four different temperatures during the dehydrogenation process. The most important result is

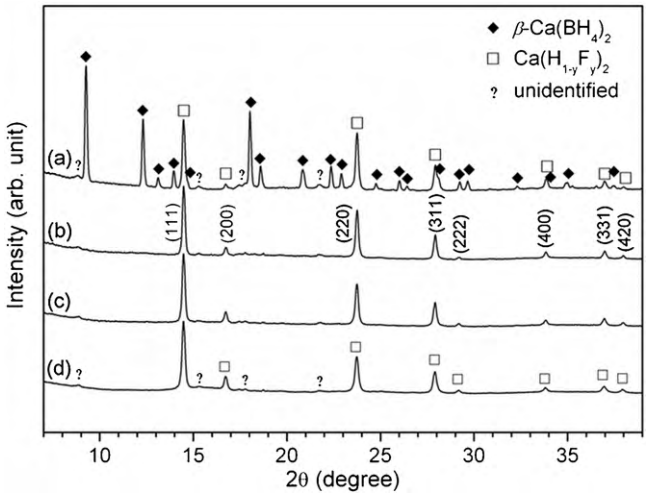

Fig. 5. In-situ synchrotron XRD patterns of **1** during the dehydrogenation process at a temperature of (a) 349 °C, (b) 354 °C, (c) 359 °C, and (d) 390 °C.

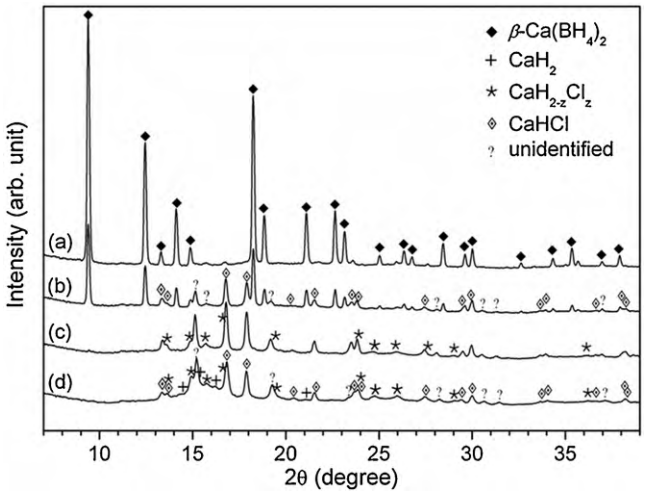

Fig. 6. In-situ synchrotron XRD patterns of **2** during the dehydrogenation process at a temperature of (a) 349 °C, (b) 354 °C, (c) 359 °C, and (d) 390 °C.

that $Ca(H_{1-y}F_y)_2$ is the major phase in the course of dehydrogenation. Both the intermediate phase and orthorhombic CaH_2 (o-CaH_2) which are the main phases in the case of pure $Ca(BH_4)_2$ [46–48] are not clearly seen. CaH_2 is stable in an orthorhombic structure (space group *Pnma*), but extensive solubility in the cubic CaF_2 structure (space group *Fm-3m*) has been reported [39]. The H fraction in the F site can be estimated from the relative peak intensities. In pure CaF_2, (2 0 0) peak is not at all seen as in Fig. 1(a). The gradual growth of (2 0 0) peak from (a) to (d) hints at increasing proportion of H in $Ca(H_{1-y}F_y)_2$ (the patterns are normalized with respect to the (1 1 1) peak intensity).

Then the question is what would be the role of CaF_2. In short, from the initial stage of dehydrogenation, CaF_2 would act as a seed for the formation of CaH_2: the presence of CaF_2 could drive $Ca(BH_4)_2$ to decompose directly into $Ca(H_{1-y}F_y)_2$ thereby changing the overall dehydrogenation pathway. The complexity of dehydrogenation pathway of $Ca(BH_4)_2$ is largely due to an elusive nature of the intermediate phase. The final dehydrogenated product is CaH_2 and CaB_6 [49], but the chemical formula of the intermediate phase is not conclusive yet [46–49]. That intermediate phase is not clearly seen during the in-situ dehydrogenation of **1**. The formation of $Ca(H_{1-y}F_y)_2$ at the initial stage of dehydrogenation, therefore, indicates that a larger part of $Ca(BH_4)_2$ may directly decompose into $Ca(H_{1-y}F_y)_2$ and CaB_6, or into $Ca(H_{1-y}F_y)_2$ and an intermediate phase of other kind. A recent structure solution [48] has suggested that the intermediate phase may not be formed together with CaH_2, i.e., B to Ca ratio is kept to two in the intermediate phase, unlike $Li_2B_{12}H_{12}$ or $MgB_{12}H_{12}$. A theoretical investigation has shown that decomposition through $CaB_{12}H_{12}$ would be slightly unfavorable compared to a direct decomposition into CaH_2 and CaB_6 [50]. These all point to an intriguing characteristic of the intermediate phase of $Ca(BH_4)_2$; a thorough experimental and theoretical investigation is much needed.

In-situ dehydrogenation process of **2** is presented in Fig. 6. The dehydrogenation proceeds in a complex sequence. In the beginning, CaHCl is formed together with unknown phase(s). The common intermediate phase is again not found as in the case of **1**. Here the role of Cl is similar to that of F. The spontaneous formation of CaHCl would provide a thermodynamic driving force to the decomposition of $Ca(BH_4)_2$ into CaH_2:

$$\frac{1}{2}CaH_2 + \frac{1}{2}CaCl_2 \rightarrow CaHCl. \quad (3)$$

As CaH_2 gradually comes out from $Ca(BH_4)_2$, new peaks that are indexed as $CaH_{2-z}Cl_z$ (Fig. 6(c)) appear, which will be explained

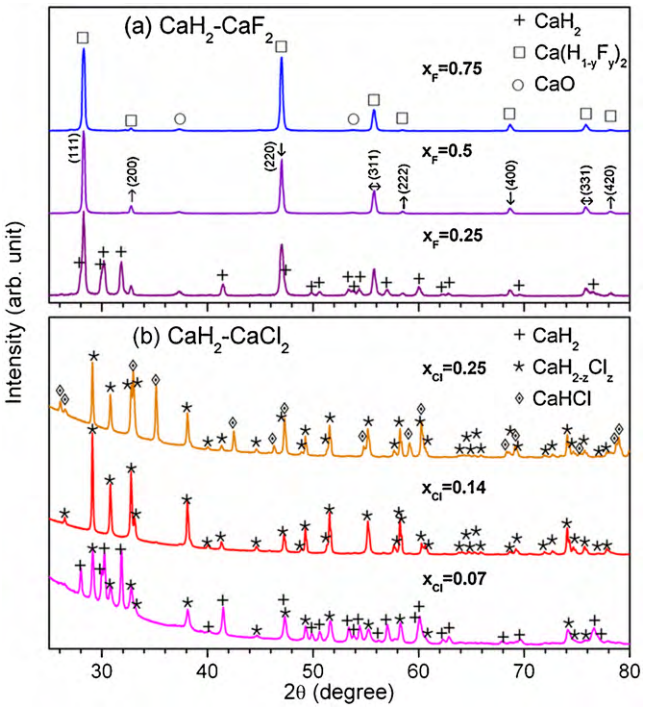

Fig. 7. XRD patterns of (a) CaH_2–CaF_2 and (b) CaH_2–$CaCl_2$ in different mixing ratio. x_F and x_{Cl} are the mole fraction of CaF_2 and $CaCl_2$ in the starting material, respectively. In the panel (a) the intensities are renormalized with respect to the (1 1 1) peak intensity. Different type of arrows indicates the change in peak intensity which grows (↑), shrinks (↓), or remains unchanged (↔) as x_F decreases.

shortly, and finally a weak signature of CaH_2 starts to be seen.

The apparent change in dehydrogenation reaction pathway relies more on a rather interesting chemistry between CaH_2 and CaX_2 in the dehydrogenated product than the change in the starting material. Therefore it is worthwhile to have a closer look at CaH_2–CaX_2 systems. We present in Fig. 7(a) and (b) the XRD patterns of CaH_2–CaF_2 and CaH_2–$CaCl_2$ mixtures in the different mixing ratios as detailed in the experimental section. In Fig. 7(a), only the peak intensities change when x_F stays within the solubility limit; separation of the orthorhombic CaH_2 phase (o-CaH_2) occurs when the content of CaH_2 is over the solubility limit. In our in-situ experiment, even after full dehydrogenation, the peaks of o-CaH_2 do not appear clearly. Since 0.9 mol of $Ca(BH_4)_2$ would produce 0.6 mol of CaH_2 according to the reaction (1), x_F will become 0.14 at the final stage. If the system remains out-of-equilibrium where all of CaH_2 exists in the cubic solid solution phase, (2 0 0) peak should be as large as 32% of the (1 1 1) peak at $x_F = 0.14$, which is definitely not the case in Fig. 5(d). So the loss of o-CaH_2 is not completely understood. Similar XRD pattern was reported previously in $Ca(BH_4)_2$–$0.02NbF_5$ [4] without a detailed explanation.

In the case of CaH_2–$CaCl_2$, our initial intention is to resolve at least some of the unidentified peaks in Fig. 6. We start from the composition $x_{Cl} = 0.14$ to mimic the situation after full dehydrogenation as mentioned above. According to the phase diagram study by Sridharan et al. [51] it would consist of CaH_2 and CaHCl at high temperatures. Instead, as shown in the second XRD pattern in Fig. 7(b) a completely different pattern appears. We are able to index most of the peaks as the peaks of a hexagonal lattice of $a = 9.375$ Å and $c = 3.697$ Å using the program TOPAS [52]. We tentatively call this phase as $CaH_{2-z}Cl_z$ with z being ca. 0.29. This rather peculiar stoichiometry would probably be linked to an interesting arrangement of H and Cl. We leave the structure identification as a future study. The XRD patterns obtained from CaH_2 and $CaCl_2$ rich side sample ($x_{Cl} = 0.07$ and 0.25, respectively) show that no new phase exists other than $CaH_{2-z}Cl_z$ between CaH_2 and CaHCl.

4.4. Thermodynamics

We have confirmed the formation of a solid solution or a compound in both the reactants and products. Then the next step is to estimate the associated enthalpy and entropy change and the subsequent dehydrogenation temperature change.

We start our discussion on the reactant side. In the case of **1**, $Ca(BH_4)_2$ and CaF_2 form a physical mixture, and therefore there is no energy change in the reactant side. For **2**, the partial molar enthalpy and entropy change upon the solid solution formation can be roughly estimated from a simple regular solution model [53]:

$$\Delta H_{\mathrm{mix}}(\mathrm{total}) = Lx(1-x), \tag{4}$$

$$\Delta H_{\mathrm{mix}}(\mathrm{Ca(BH_4)_2}) = Lx^2, \tag{5}$$

$$\Delta S_{\mathrm{mix}}(\mathrm{Ca(BH_4)_2}) = -2R\ln(1-x), \tag{6}$$

where L is a fitting parameter and x is the mole fraction of $CaCl_2$. Referring to Table 1, $\Delta H_{\mathrm{mix}}(\mathrm{total}) = 0.5$ kJ/mol and $x = 0.1$ gives ΔH_{mix} ($Ca(BH_4)_2$) and ΔS_{mix} ($Ca(BH_4)_2$) about 0.056 kJ/mol and 1.75 J/K mol, respectively. From a DFT study, the enthalpy and entropy of the reaction (1) is 40.6 kJ/mol H_2 and 109.3 J/K mol H_2 [49]. When ΔH_{mix} and ΔS_{mix} are taken into account, the decomposition temperature obtained from $T = \Delta H/\Delta S$ slightly increases by 1.6 °C. This is expected since the activity of $Ca(BH_4)_2$ will be smaller in the solid solution, implying stabilization of $Ca(BH_4)_2$. In the product side, the reaction between CaH_2 and CaX_2 would lower the decomposition temperature. For **2**, ΔH and ΔS of the formation of CaHCl as in the reaction (3) are −4.4 kJ and −5.7 J/K per mol CaHCl at 25 °C. We are not able to include $CaH_{2-z}Cl_z$ at the moment since the structure is yet unknown.

Similarly, we can consider the following reaction for **1**:

$$\frac{1}{2}o\text{-}\mathrm{CaH_2} + \frac{1}{2}\mathrm{CaF_2} \rightarrow \mathrm{Ca(H_{0.5}F_{0.5})_2}. \tag{7}$$

Since the solid solution takes a cubic symmetry, phase transformation from orthorhombic to cubic CaH_2 (c-CaH_2) should first be taken into account; $\Delta H(o \rightarrow c)$ and $\Delta S(o \rightarrow c)$ are 6.6 kJ/mol and 0.6 J/K mol, respectively. Then, the enthalpy of mixing of the reaction,

$$(1-y)c\text{-}\mathrm{CaH_2} + y\mathrm{CaF_2} \rightarrow \mathrm{Ca(H_{1-y}F_y)_2} \tag{8}$$

was calculated at several compositions (details in Table S3 in the supplementary data) and was fitted to the following equation [54]:

$$\Delta H_{\mathrm{mix}} = y(1-y)(L_0 + L_1(2y-1) + L_2(2y-1)^2), \tag{9}$$

where L_is are fitting parameters. ΔS_{mix} was evaluated using Eq. (2), again assuming a regular solution behavior. The results are summarized in Fig. 8. ΔH and ΔS of the reaction (7) are 3.9 kJ and 11.8 J/K per mol $Ca(H_{0.5}F_{0.5})_2$ at 25 °C. Our DFT calculation correctly predicts the solid solution formation at 400 °C.

When ΔH and ΔS of the reactions (3) and (7) are incorporated, the equilibrium temperature of the following reaction:

$$9\mathrm{Ca(BH_4)_2} + \mathrm{CaX_2} \leftrightarrow 2\mathrm{CaHX} + 5\mathrm{CaH_2} + 3\mathrm{CaB_6} + 30\mathrm{H_2} \tag{10}$$

decreases by 0.3 °C for **1** and 1.4 °C for **2**. The reaction (10) is an overall reaction, but in the early stage the reaction would rather proceed as follows:

$$\frac{3}{2}\mathrm{Ca(BH_4)_2} + \mathrm{CaX_2} \leftrightarrow 2\mathrm{CaHX} + \frac{1}{2}\mathrm{CaB_6} + 5\mathrm{H_2}. \tag{11}$$

Then the temperature decrease will be 1.8 °C for **1** and 8.6 °C for **2**. We would like to note that CaF_2 could be more effective in the

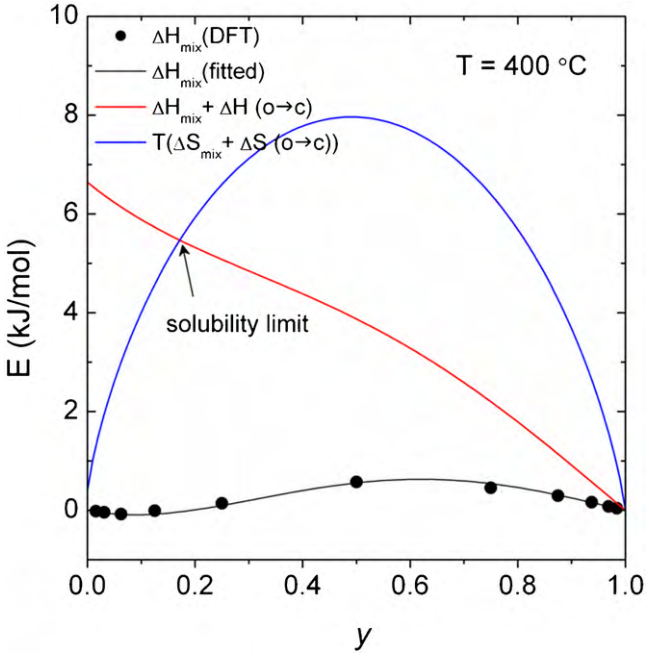

Fig. 8. Enthalpy and entropy of the $Ca(H_{1-y}F_y)_2$ system.

very early stage since the partial molar free energy of CaH_2 in $Ca(H_{1-y}F_y)_2$ would diverge to a negative infinity when y is close to one. However, such a strong driving force would rapidly diminish as the mole fraction of CaH_2 increases.

In summary, the overall thermodynamic modification is minor, and the dehydrogenation temperature would decrease by ~10 °C at most. Thus, change in the decomposition pathway is the major effect of CaX_2 addition and it is worthy of more attention including possible change in reversibility. Transition metal halides are known to be very effective catalytic precursors in the rehydrogenation process and that effect could also come from the halide ions, not solely from the transition metal elements. [4,21,26,55].

5. Conclusions

We have investigated dehydrogenation characteristics of $Ca(BH_4)_2$ in the presence of CaF_2 and $CaCl_2$. Our experiments and calculations consistently find dissolution of $CaCl_2$ into $Ca(BH_4)_2$ and phase separation between CaF_2 and $Ca(BH_4)_2$. These $Ca(BH_4)_2$–CaX_2 composites exhibit different dehydrogenation pathway, in which the typical intermediate phase of pure $Ca(BH_4)_2$ is not clearly seen. The formation of a solid solution or a compound between CaH_2 and CaX_2 may be responsible for such a change; a new compound $CaH_{2-z}Cl_z$ ($z \sim 0.29$) is found. The overall change in thermodynamics introduced by CaX_2 is estimated by first-principles calculation and turns out not to be significant. Further work should focus on the change in the rehydrogenation pathway brought by halide ions, which has not been extensively investigated so far.

Acknowledgements

This work has been sponsored by the Hydrogen Energy R&D Center, one of 21st Century Frontier R&D Programs funded by the Ministry of Education, Science and Technology of Korea. The authors gratefully acknowledge the support by Ik Jae Lee and Keun Hwa Chae at the KIST-PAL beamline.

Appendix A. Supplementary data

Supplementary data associated with this article can be found, in the online version, at doi:10.1016/j.jallcom.2010.07.051.

References

[1] L. Schlapbach, A. Züttel, Nature 414 (2001) 353–358.
[2] J.J. Vajo, T.T. Salguero, A.F. Gross, S.L. Skeith, G.L. Olson, J. Alloys Compd. 446–447 (2007) 409–414.
[3] S.V. Alapati, J.K. Johnson, D.S. Sholl, Phys. Chem. Chem. Phys. 9 (2007) 1438–1452.
[4] J.-H. Kim, J.-H. Shim, Y.W. Cho, J. Power Sources 181 (2008) 140–143.
[5] D. Ravnsbæk, Y. Filinchuk, Y. Cerenius, H.J. Jakobsen, F. Besenbacher, J. Skibsted, T.R. Jensen, Angew. Chem. Int. Ed. 48 (2009) 6659–6663.
[6] J.S. Hummelshøj, et al., J. Chem. Phys. 131 (2009) 014101.
[7] L.M. Arnbjerg, D.B. Ravnsbæk, Y. Filinchuk, R.T. Vang, Y. Cerenius, F. Besenbacher, J.-E. Jørgensen, H.J. Jakobsen, T.R. Jensen, Chem. Mater. 21 (2009) 5772–5782.
[8] H. Oguchi, M. Matsuo, J.S. Hummelshoj, T. Vegge, J.K. Norskov, T. Sato, Y. Miura, H. Takamura, H. Maekawa, S. Orimo, Appl. Phys. Lett. 94 (2009) 141912.
[9] L. Mosegaard, B. Møller, J.-E. Jørgensen, Y. Filinchuk, Y. Cerenius, J.C. Hanson, E. Dimasi, F. Besenbacher, T.R. Jensen, J. Phys. Chem. C 112 (2008) 1299–1303.
[10] L. Yin, P. Wang, Z. Fang, H. Cheng, Chem. Phys. Lett. 450 (2008) 318–321.
[11] H. Maekawa, M. Matsuo, H. Takamura, M. Ando, Y. Noda, T. Karahashi, S.I. Orimo, J. Am. Chem. Soc. 131 (2009) 894–895.
[12] C.E. Messer, J. Mellor, J. Phys. Chem. 64 (1960) 503–505.
[13] C.E. Messer, J. Solid State Chem. 2 (1970) 144–155.
[14] E.H. Majzoub, J.L. Herberg, R. Stumpf, S. Spangler, R.S. Maxwell, J. Alloys Compd. 394 (2005) 265–270.
[15] L.-C. Yin, P. Wang, X.-D. Kang, C.-H. Sun, H.-M. Cheng, Phys. Chem. Chem. Phys. 9 (2007) 1499–1502.
[16] H.W. Brinks, A. Fossdal, B.C. Hauback, J. Phys. Chem. C 112 (2008) 5658–5661.
[17] N. Eigen, U. Bösenberg, J. Bellosta von Colbe, T.R. Jensen, Y. Cerenius, M. Dornheim, T. Klassen, R. Bormann, J. Alloys Compd. 477 (2009) 76–80.
[18] G.B. Wilson-Short, A. Janotti, A. Peles, C.G. Van de Walle, J. Alloys Compd. 484 (2009) 347–351.
[19] J.J. Vajo, S.L. Skeith, F. Mertens, J. Phys. Chem. B 109 (2005) 3719–3722.
[20] X.-D. Kang, P. Wang, L.-P. Ma, H.-M. Cheng, Appl. Phys. A 89 (2007) 963–966.
[21] E. Rönnebro, E.H. Majzoub, J. Phys. Chem. B 111 (2007) 12045–12047.
[22] E. Jeon, Y.W. Cho, J. Alloys Compd. 422 (2006) 273–275.
[23] H.-W. Li, S. Orimo, Y. Nakamori, K. Miwa, N. Ohba, S. Towata, A. Züttel, J. Alloys Compd. 446 (2007) 315–318.
[24] S.-A. Jin, Y.-S. Lee, J.-H. Shim, Y.W. Cho, J. Phys. Chem. C 112 (2008) 9520–9524.
[25] F.E. Pinkerton, M.S. Meyer, J. Alloys Compd. 464 (2008) L1–L4.
[26] J.-H. Kim, S.-A. Jin, J.-H. Shim, Y.W. Cho, Scr. Mater. 58 (2008) 481–483.
[27] A.P. Hammersley, S.O. Svensson, M. Hanfland, A.N. Fitch, D. Häusermann, High Press. Res. 14 (1996) 235–248.
[28] J.P. Perdew, K. Burke, M. Ernzerhof, Phys. Rev. Lett. 77 (1996) 3865–3868.
[29] M.C. Payne, M.P. Teter, D.C. Allan, T.A. Arias, J.D. Joannopoulos, Rev. Mod. Phys. 64 (1992) 1045–1097.
[30] P. Giannozzi, et al., J. Phys.: Condens. Matter 21 (2009) 395502.
[31] http://www.quantum-espresso.org.
[32] D. Vanderbilt, Phys. Rev. B 41 (1990) 7892–7895.
[33] S. Baroni, S. de Gironcoli, A. Dal Corso, P. Giannozzi, Rev. Mod. Phys. 73 (2001) 515–562.
[34] CRC Handbook of Chemistry and Physics, 86th ed., CRC Press, 2005–2006.
[35] H. Mo, T.C. Pochapsky, J. Phys. Chem. B 101 (1997) 4485–4486.
[36] A.L. Verma, J. Van Der Elsken, J. Phys. Chem. Solids 38 (1977) 5–8.
[37] P.-O. Löwdin, J. Chem. Phys. 18 (1950) 365–375.
[38] M. Fichtner, K. Chłopek, M. Longhini, H. Hagemann, J. Phys. Chem. C 112 (2008) 11575–11579.
[39] J.-F. Brice, A. Courtois, J. Aubry, J. Solid State Chem. 24 (1978) 381–387.
[40] Y. Fukai, The Metal–Hydrogen System, 2nd ed., Springer, Berlin, 2005.
[41] K. Miwa, M. Aoki, T. Noritake, N. Ohba, Y. Nakamori, S. Towata, A. Züttel, S. Orimo, Phys. Rev. B 74 (2006) 155122.
[42] Y.-S. Lee, Y. Kim, Y.W. Cho, D. Shapiro, C. Wolverton, V. Ozolins, Phys. Rev. B 79 (2009) 104107.
[43] T.H. Jordan, B. Dickens, L.W. Schroeder, W.E. Brown, Acta Crystallogr. B 31 (1975) 669–672.
[44] G. Barkhordarian, T.R. Jensen, S. Doppiu, U. Bösenberg, A. Borgschulte, R. Gremaud, Y. Cerenius, M. Dornheim, T. Klassen, R. Bormann, J. Phys. Chem. C 112 (2008) 2743–2749.
[45] J.Y. Lee, D. Ravnsbæk, Y.-S. Lee, Y. Kim, Y. Cerenius, J.H. Shim, T.R. Jensen, N.H. Hur, Y.W. Cho, J. Phys. Chem. C 113 (2009) 15080–15086.
[46] J.-H. Kim, S.-A. Jin, J.-H. Shim, Y.W. Cho, J. Alloys Compd. 461 (2008) L20–L22.
[47] M. Aoki, K. Miwa, T. Noritake, N. Ohba, M. Matsumoto, H.-W. Li, Y. Nakamori, S. Towata, S. Orimo, Appl. Phys. A 92 (2008) 601–605.
[48] M.D. Riktor, M.H. Sørby, K. Chłopek, M. Fichtner, B.C. Hauback, J. Mater. Chem. 19 (2009) 2754–2759.
[49] Y. Kim, D. Reed, Y.-S. Lee, J.Y. Lee, J.-H. Shim, D. Book, Y.W. Cho, J. Phys. Chem. C 113 (2009) 5865–5871.

[50] V. Ozolins, E.H. Majzoub, C. Wolverton, J. Am. Chem. Soc. 131 (2009) 230–237.
[51] R. Sridharan, K.H. Mahendran, T. Gnanasekaran, G. Periaswami, U.V. Varadaraju, C.K. Mathews, J. Nucl. Mater. 223 (1995) 72–79.
[52] TOPAS version 4.1, Bruker AXS GmbH, Karlsruhe, Germany, 2003–2008.
[53] D.R. Gaskell, Introduction to the Thermodynamics of Materials, 3rd ed., Taylor & Francis, 1995.
[54] O. Redlich, A.T. Kister, Ind. Eng. Chem. 40 (1948) 345–348.
[55] C. Rongeat, V. D'Anna, H. Hagemann, A. Borgschulte, A. Züttel, L. Schultz, O. Gutfleisch, J. Alloys Compd. 493 (2010) 281–287.